Indian Journal of Pure & Applied Physics
Vol. 61, February 2023, pp. 132-139
DOI: 10.56042/ijpap.v61i2.67097

Effect of Passivation Layers Permittivity on DC and RF Parameters of GaN MESFETs

N Abdaoui[a], I Hadjoub[a, b*], A Doghmane[a], L Abid[a] & Z Hadjoub[a]

[a]Laboratoire des Semi-conducteurs, Département de Physique, Faculté des Sciences, Université Badji-Mokhtar, Annaba, B.P 12, DZ-23000 Algeria.

[b]ÉcoleNationale Supérieure deTechnologie et d'Ingénierie, ENSTI, Annaba, DZ-23000, Algeria.

Received 3 October 2022; accepted 18 January 2023

Surface passivation impact on DC and RF characteristics of GaN MESFETs was studied using ATLAS simulator from Silvaco. It has been shown that when the relative permittivity, ε_r, of the inter-electrode passivation layers increases, the breakdown voltage as well as the maximum output power density increases thus improving the applications of the MESFET device in high voltage and high power. However, the high values of relative permittivity lead to an increase in the gate-source C_{GS} and gate-drain C_{GD} capacitances on which the radio frequency performance of GaN MESFET transistors depends strongly. In effect, this increase leads to a limitation of the performances, RF of the GaN MESFET transistors. Finally, the variations of the parameters studied as a function of ε_r have been quantified and mathematical expressions are established. These formulas can be very useful for the judicious choice of the passivation layer in GaN MESFETs.

Keywords: GaN MESFET; DC and RF parameters; Breakdown voltage; Power density; Access capacitances

1 Introduction

Nowadays, the Metal Semiconductor Field Effect Transistor, MESFET, is a highly investigated unipolar electronic device, in particular, for power and microwave applications such as oscillators and amplifiers. The great interest of research work in MESFET structures[1-4] is the result of the ease of their fabrication and consequently their introduction in large-scale integrated circuits. It is well established that high power devices require the use of semiconductor materials supporting very strong electric fields. The most suitable semiconductors for such a purpose are those characterized by large energy gaps, E_g, (generally $E_g > 3$ eV) such as SiC and GaN which have all the desired properties to the fabrication of high quality electronic devices.

In fact, in recent years, it has been shown that GaN electronic devices offer good performances as far as breakdown voltage, power density, high temperature and low on-state resistance are concerned[5-9]. In addition to its large gap of about 3.4 eV and its high critical field, GaN is characterized by a high electron mobility and a high saturation velocity, which improve the switching frequency and thermal generation rate. These properties, combined with good thermal conductivity, good stability and high melting point, make GaN an attractive material for high temperature and high power devices such as in MESFETs that are suitable for operation in tough environments[10-13].

Furthermore, passivation is an essential technological step in the design of semiconductor devices. It stabilizes surface electrical states during device operations. It also reduces the effect of external contamination (moisture and/or other impurities), which would degrade the device electrical characteristics with time, including GaN MESFETs. In this context, we investigate the effect of the relative permittivity of passivation layers on direct current, DC, and radio frequency, RF, of GaN MESFETs. To do so, two-dimensional numerical simulations of the device's performance were carried out using ATLAS of Silvaco physical simulator. Thus, DC and RF performances are investigated for such devices with different passivation layers: SiO_2, Si_3N_4, Al_2O_3, $HfSiO_4$,Gd_2O_3, Y_2O_3, Ta_2O_5, ZrO_2, HfO_2, La_2O_3 and TiO_2.

2 MODELS in ATLAS for GaN Structures

Numerical simulations were performed using ATLAS of Silvaco software[14]. This simulator permits the prediction of the DC, AC or transient electrical characteristics of semiconductor devices. In addition

*Corresponding author: (E-mail: i.hadjoub@esti-annaba.dz)

to electrical behavior, it provides information about the internal distribution of electrical variables such as field lines. The investigated device is considered as a mesh structure where each node has typical properties such as: material type, doping type, dopant concentration, *etc*. Note that electrodes are represented by surfaces on which the bias voltages are applied. Hence, for each node, the concentration of carriers, the electric field, the current, etc. can be obtained through the resolution of the fundamental device equations: transport equations, continuity equations and Poison's equation.

The main physical models used in the present study include the Shockley Read-Hall (SRH) and Auger recombination processes, incomplete doping activation, impact ionization, carrier mobility as a function of doping. The essentials of these different processes and models are recalled below:

***SRH and Auger recombination processes*:** Carrier generation-recombination is the process by which the semiconductor material returns to equilibrium after perturbation. In the ATLAS simulator, two models are implemented for these recombination mechanisms: (i) the SRH recombination model which is the most dominant recombination process for MESFET transistors and (ii) the Auger recombination which is the dominant process at high doping levels.

***Incomplete Ionization*:** GaN is doped with silicon, Si, as a donor and magnesium, Mg, as an acceptor, both of which possess high activation energies and are not completely ionized even at high temperature in particular for p type[15] materials. Thus, proper modelling of incomplete ionization becomes extremely important.

***Impact Ionization*:** As the applied voltage increases, the electrical field in the channel increases, causing the moving carriers to move at higher velocities. At this sufficiently high electric field, carriers acquire sufficient kinetic energy that leads to impact ionization or avalanche effect, leading to a cascade of mobile carriers transported through the depopulation region giving rise to a significant current flow. Note that the rapid increase in current and the lack of control of this effect can lead to an irreversible device breakdown.

***Band-to-Band Tunneling*:** When an electric field is sufficiently high inside a device, a local band curvature would be sufficient to generate an electron–hole pair. This generation mechanism is introduced in the right hand side of the continuity equations.

Electron and Hole Mobility: Unlike silicon, GaN has a negative differential mobility for electrons at very high fields. Thus, for GaN, a dual mobility model approach is adopted: (i) one for the positive differential region at low field and (ii) the other for the negative differential region at high field. The Caughey–Thomas mobility model, modified by Farahmand (FMCT), consisting of low and high field mobility models is chosen.

It should be noted that GaN parameters vary considerably with crystalline structures, layers orientation and growth techniques. GaN crystallizes in two different structures: (i) cubic polytype (zinc blend structure: c-GaN), which is thermodynamically metastable and (ii) hexagonal phase (wurtzite structure: h-GaN) which is a thermodynamically stable polytype. The wurtzite GaN important parameters, chosen in this simulation, are grouped in Table 1.

3 GaN MESFETs Structure

Figure 1 illustrates a cross section of a typical gallium nitride MESFET used in the present work. A semi-insulating substrate of n-type GaN, weakly doped with Si is considered over which a buffer p-type layer, weakly doped with magnesium, is deposited. The next n-type layer is slightly doped with Si to represent the conductive channel. Then, three contacts are deposited: The gate electrode, G, of Schottky type, is positioned in the middle, whereas the source, S, and drain, D, electrodes, which are ohmic contacts, are positioned on either side of the gate. To improve the ohmic contacts; two heavily doped thin zones of n^+ type are introduced underneath S and D contacts. Finally, to protect the device from external effects, a passivation layer is added between all contacts. The dimensions and values of geometric and technological parameters of the present GaN MESFET structure are grouped in Table 2.

The fundamental parameter that characterizes a passivation insulating layer is its relative permittivity, ε_r. To quantify the influence of this parameter on the characteristics of the GaN MESFET, we considered

Table 1 — Fundamental parameters of wurtzite GaN.s

Parameter	Symbol	Value
Energy gap	E_g	3.4 eV
Electronicaffinity	χ	4.31 eV
Relative permittivity	ε_r	8.9
Electron mass in vacuum	m_0	9,1094 10^{-28}g
Effective electron mass	m_e	0.2 m_0
Effective hole mass	m_p	0.15 m_0

several insulators(SiO_2, Si_3N_4, Al_2O_3, $HfSiO_4$,Gd_2O_3, Y_2O_3, Ta_2O_5, ZrO_2, HfO_2, La_2O_3 andTiO_2) with different ε_r values ranging from 3.9 (for SiO_2) to 80 (for TiO_2). Moreover, to enrich this investigation and in order to cover a wide and continuous range of ε_r values, we considered some fictitious dielectric materials, D_x, with a chosen permittivity, denoted: D_1, D_2, D_3, D_4 and D_5. Both real and fictitious materials data are grouped in Table 3.

4 Electrical Field Distributions

The distribution of electric fields along an electronic device is of great importance for any specific application. In fact, the electric field is very inhomogeneous in III-V semiconductors devices. Therefore, it is necessary to take into account this effect in order to avoid premature breakdown in the zones subjected to a strong electric field. To better understand the origin of this phenomenon, we study the two-dimensional distribution of electric field lines in GaN MESFET using ATLAS simulator from Silvaco.

4.1 Highlighting the Phenomenon

Figure 2 shows the two-dimensional distribution of the electric field lines in the GaN MESFET at a drain bias, V_{DS}= 40 V and agate voltage, V_{GS} = 0 V for two different passivation layers(a) SiO_2, and (b) HfO_2. It can clearly be seen that in the channel, at the gate edge facing the drain, at the device surface, there is a dense accumulation of electric field lines because the potential difference between the gate and the drain is greater than that between the gate and the source. The channel near the drain is therefore narrower than that

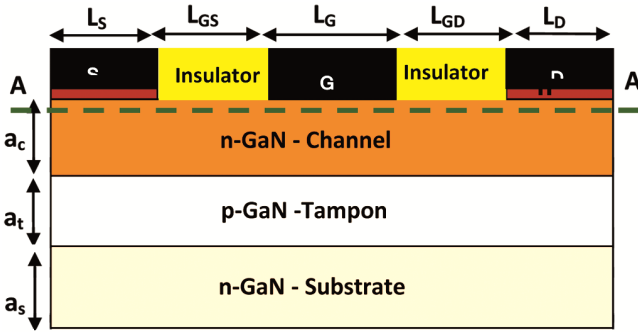

Fig. 1 — Cross section of GaN MESFET.

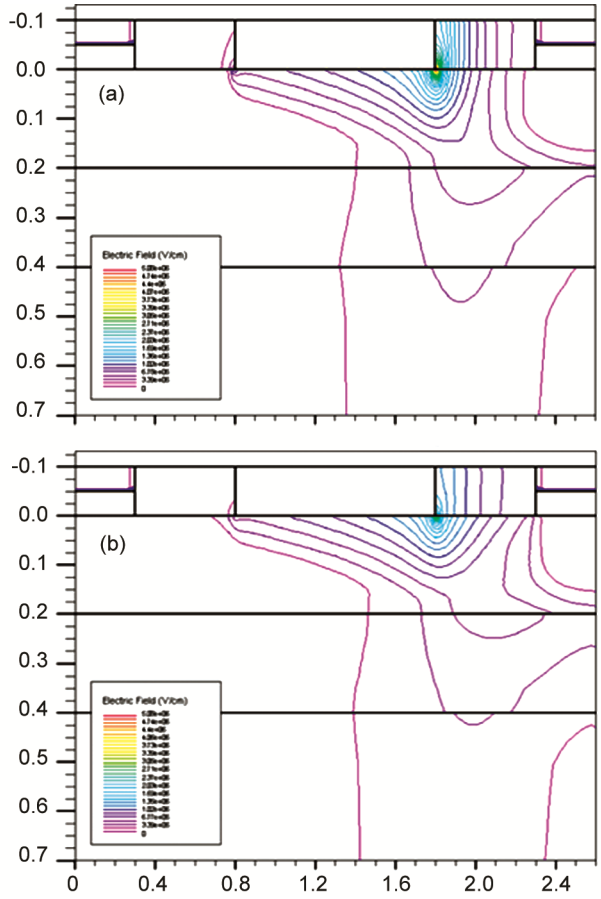

Fig. 2 — Two-dimensional distribution of the electric field lines in the GaN MESFET with (a) $SiO_2$and (b) HfO_2passivation layers at V_{DS}= 40 V and V_{GS}= 0V.

Table 2 — Values of geometric and technological parameters of the GaN MESFET structures

Parameter	Symbol	Value
Gate length	L_G	1.0 µm
Drain length	L_D	0.3 µm
Source length	L_S	0.3 µm
Gate - source spacing	L_{GS}	0.5 µm
Gate - drain spacing	L_{GD}	0.5 µm
Channel height	a_c	0.2 µm
Substrate height	a_s	0.3 µm
buffer layer height	a_t	0.2 µm
Doping concentration of channel region	N_D	$3.10^{17}cm^{-3}$
Doping concentration of regions under source and drain	n^+	$2.10^{19}cm^{-3}$
Doping concentration of buffer region	N_A	$1.4.10^{15}cm^{-3}$
Doping concentration of substrate region	N_S	$1.10^{14}cm^{-3}$
Metal gate work function	ϕ_m	5.1 eV

Table 3 — Values of relative permittivity of real[16-18]and fictitious passivation layers, $Dx_{(1-5)}$

Insulator	D_1	SiO_2	Si_3N_4	Al_2O_3	$HfSiO_4$	Gd_2O_3	Y_2O_3	Ta_2O_5	ZrO_2	HfO_2	La_2O_3	D_2	D_3	D_4	D_5	TiO_2
ε_r	2	3.9	7.5	9	11	12	15	22	23	25	30	40	50	60	70	80
Ref.	-	[16]	[16]	[17]	[17]	[18]	[17]	[17]	[18]	[17]	[17]	-	-	-	-	[17]

neighboring the source side. It can also be noted that at under the same previous polarization.

conditions, the structure with the hafnium oxide passivation layer Fig. 2(b) presents less dense field lines than the structure with the silicon oxide passivation layer. Hence, it would be interesting to carry out a deeper analysis in order to quantify this phenomenon.

4.2 Phenomenon Quantification

Figure 3 shows the electrical field distribution of the GaN MESFET structure, at the cut line AA' located at a distance of 0.1 nm from the channel surface (Fig. 1) obtained at V_{DS}= 40 V and V_{GS} = 0 V for different passivation layers: TiO_2, La_2O_3, HfO_2, ZrO_2, Ta_2O_5, Y_2O_3, Gd_2O_3, $HfSiO_4$, Al_2O_3, Si_3N_4, and SiO_2. It can be seen that several very sharp peaks are obtained at the same location; these peaks represent the maximum reached electric field due to the high voltage at the gate edge neighboring the drain. Moreover, the intensity of these peaks depends on the type of passivation dielectric layers (insert to Fig. 3). Therefore, it would be interesting to quantify this dependence by the relative permittivity of such layers.

Hence, we plot in Fig. 4, the maximum peak intensity value of the electric field as a function of the relative permittivity of the investigated passivation layers in the present GaN MESFET, at V_{GS} = 0V and V_{DS} = 40V. It can clearly be seen that the maximum peak of electric field decreases with increasing the relative permittivity. A close analysis of this behavior shows that the curve initially decreases very sharply (for $\varepsilon_r \leq 20$) then tends towards a saturation regime beyond $\varepsilon_r > 20$. Using a method of approximation, we quantified the evolution of the maximum value of the electric field as a function of relative permittivity to find an exponential decrease given the following relation:

$$E_{max}\ (\mu V/cm) = 2.5 + 3e^{-\varepsilon_r/12} \quad \ldots (1)$$

5 Breakdown Voltage

The breakdown voltage, V_{BR}, of a MESFET represents the voltage applied between the drain and the source of the device from which it reaches the breakdown region. It is expressed by an exponential increase in the drain current, thus causing irreversible damage to the device. In fact, the breakdown voltage is an important characteristic parameter whose value can constitute a serious limitation to the device performances for high voltage and high power applications. Therefore, its determination is of great importance. On the other hand, passivation is an essential technological step in the design of semiconductor devices.

Hence, we investigate the effect of the relative permittivity of the insulators used as a passivation layer on the breakdown voltage of the GaN MESFET. The obtained results, for different passivation layers (TiO_2, La_2O_3, HfO_2, ZrO_2, Ta_2O_5, Y_2O_3, Gd_2O_3, $HfSiO_4$, Al_2O_3, Si_3N_4, and SiO_2), are shown in terms of drain current Fig. 5(a) and gate current Fig. 5(b) as a function of the drain voltage at V_{GS} = 0 V. It is clear

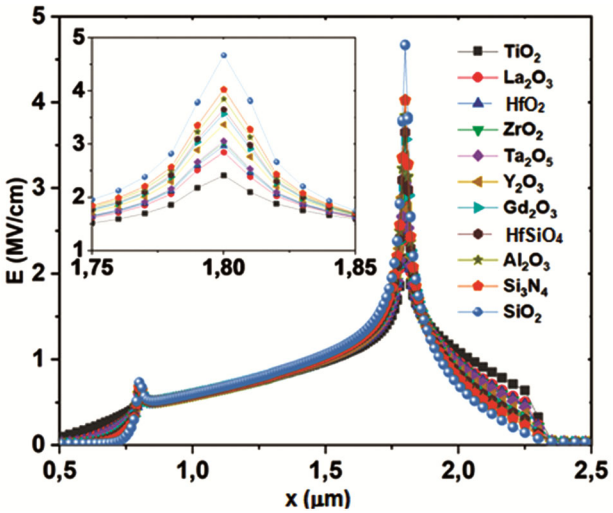

Fig. 3 — Electrical field distribution at AA' cut line by the side of a distance of 0.1 nm from the surface for different passivation layers, at V_{DS} = 40 V and V_{GS}= 0 V.

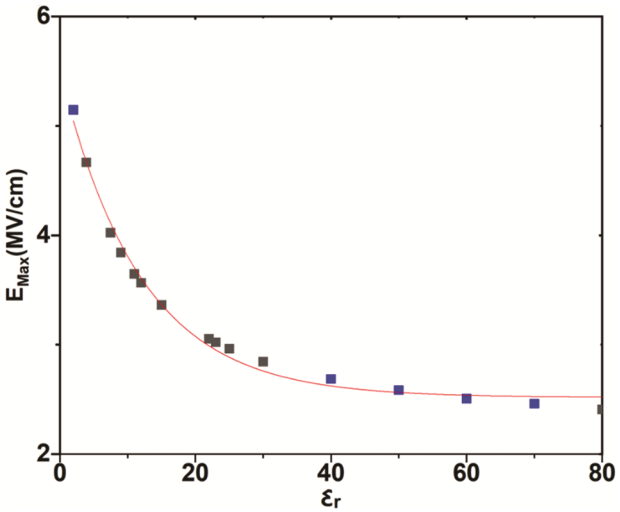

Fig. 4 — Variation of the maximum intensity of electric field in the channel in GaN MESFET as a function of relative permittivity, at V_{GS} = 0 V and V_{DS} = 40 V, forreal (■■■) and fictitious (■■■) passivation layers and the line of best fit (——).

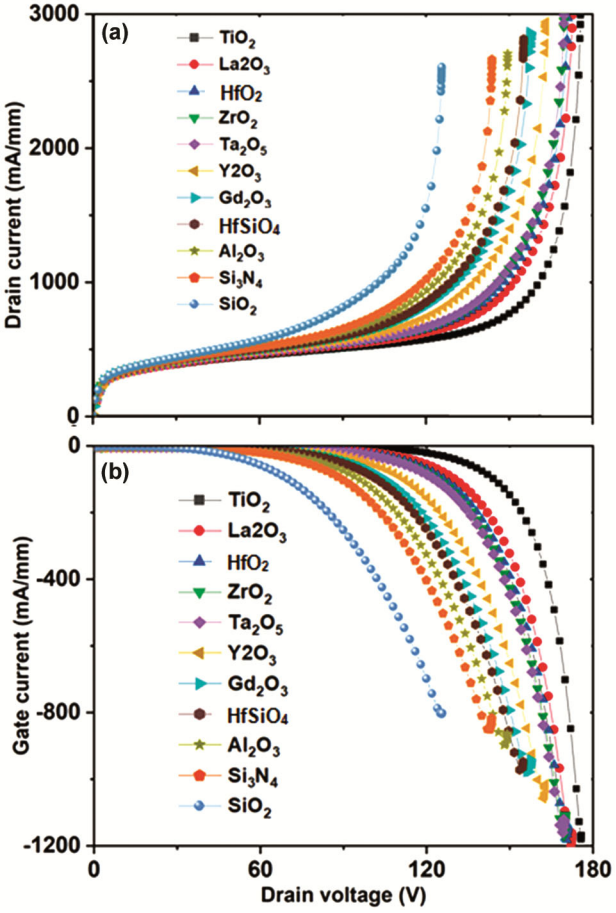

Fig. 5 — Breakdown characteristics at V_{GS} = 0 V of GaN MESFET for different passivation layers: (a) I_{DS} *vs* V_{DS} and (b) I_{GS} *vs* V_{DS}.

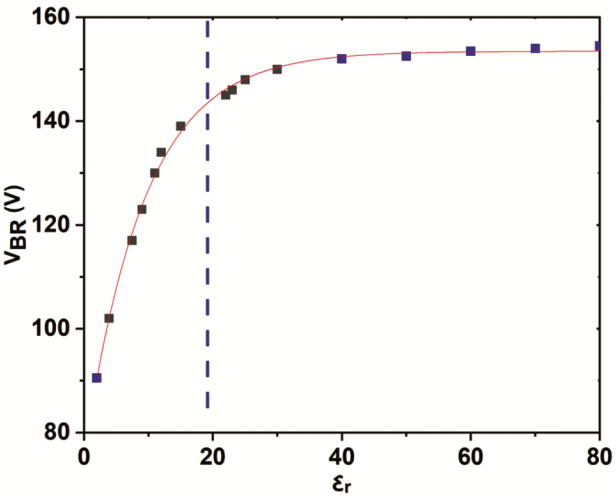

Fig. 6 — V_{BR} variations as a function of relative permittivity at V_{GS}= 0V of real (■■■) and fictitious (■■■) materials and line of best fit (——).

that, for all types of insulators, when the drain voltage increases, the drain current as well as the gate current increase exponentially, in absolute values, leading to device breakdown. This phenomenon, attributed to the ionization impact, makes it possible to determine the breakdown voltage. Note that in all cases, for $V_{DS}<V_{BR}$, the gate current is negligible. It can also be noted that the appearance of the onset of the rapid increase in current, *i.e.*, the onset of the breakdown voltage depends on the insulator type and consequently on its fundamental characteristics, mainly its relative permittivity.

In order to understand and quantify the effect of passivation layers on the breakdown voltage, we consider the relative permittivity of each investigated insulating material (Table 3). Then, we plot in Fig. 6 V_{BR} variations of the GaN MESFET as a function of the relative permittivity of the passivation layers at V_{GS}= 0 V. It can clearly be seen that as the relative permittivity increases the breakdown voltage initially increases very sharply for $\varepsilon_r \leq$ 20, then saturates beyond this value. This behavior can be explained by the fact that the breakdown occurs when the peak of the electric field in the channel area reaches its maximum, which appears at the edge of the gate next to the drain, at the device surface (Fig. 2), where the electric field lines are densely accumulated. Moreover, the peak of the electric field is reduced when the relative permittivity becomes higher. Therefore, it becomes possible to apply much higher voltages so that the electric field is equal to its critical quantity or maximum value. Thus, the device can tolerate much higher voltages and thus an improvement in breakdown voltage.

The evolution of V_{BR} as a function ε_r illustrated in Fig. 6 is quantified through curve fitting of the plotted results of real (■■■) and fictitious (■■■) passivation materials; the line of best fit (——) led to the following relation:

$$V_{BR}(V) = 153.5 - 80e^{(-\varepsilon_r/9)} \quad \ldots (2)$$

The improvement of the breakdown voltage with the use of high relative permittivity insulators is accompanied by a slight decrease of the intensity of saturation current, I_{Dsat}. Therefore, a compromise is needed even that the increase in V_{BR} is much greater than the decrease in I_{Dsat}. In order to better estimate the weighting, we consider the theoretical maximum output power density, P_{max}, which strongly depends on the intensity of the saturation current and the breakdown voltage[19-21]. This parameter is given by:

$$P_{max} = \frac{I_{Dsat}(V_{BR}-V_{Knee})}{8} \quad \ldots (3)$$

Where V_{knee} is the knee voltage. The calculated maximum output power density, at V_{GS} = 0 V and V_{DS}= 20 V, is plotted in Fig. 7 as a function of the relative permittivity of real (■■■) and fictitious (■■■) passivation materials. It can clearly be seen that the relative permittivity initially increases very sharply then saturates beyond ε_r> 20. This behavior is similar that observed above, in Fig. 6, for V_{BR} = f(ε_r). The quantification of P_{max} = f(ε_r) results (——) led to the following relation:

$$p_{max} = 6.9 - 3.5\, e^{(-3\varepsilon_r/23)} \quad \ldots (4)$$

6 Access Capacitances

Radio frequency performances of a transistor can be enhanced through the improvement of some parameters such as the cut-off frequency, f_T, and the maximum oscillation frequency, f_{max}. These parameters are inversely proportional to both gate-source capacitance, C_{GS}, and gate-drain capacitance, C_{GD}. Therefore, the reduction of C_{GS} and C_{GD} leads to the improvement of transistors RF performances. Hence, to put into evidence such a phenomenon, we plot in Fig. 8 the obtained results, at a drain voltage V_{DS} = 40 V and a frequency, f = 1 GHz, of the variation of C_{GS} and C_{GD} capacitances as a function of the gate-source voltage for different relative permittivity of the passivation layers. It can clearly be seen that the values of both capacitances increase with increasing V_{GS}.

Moreover, it can also be noted that the values of both C_{GS} and C_{GD} capacitances depend on the dielectric materials and consequently on their relative permittivity. In order to quantify such dependences we represent the evolution of C_{GD} capacitance Fig. 9(a) and C_{GS} capacitance Fig. 9(b) as a function of the relative permittivity, deduced for real and fictitious dielectrics, at V_{DS}= 40 V, f = 1 GHz and different gate polarizations V_{GS}= 0 V, -2V, -4 V, and -10 V.

We note that for all V_{GS} values, both C_{GD} and C_{GS} increase with increasing the relative permittivity. However, we can notice that the effect of ε_r on C_{GD} is linear while it is exponential on C_{GS}. Thus, to quantify these behaviors, we determined, through curve fitting, the relationships between capacitances and relative permittivity.

Hence, for the linear C_{GD} variations, the same slope of 0.18 was obtained, to give the following relation:

$$C_{GD}(10^{-5}pF/\mu m) = 0.18\varepsilon_r + \beta \quad \ldots (5)$$

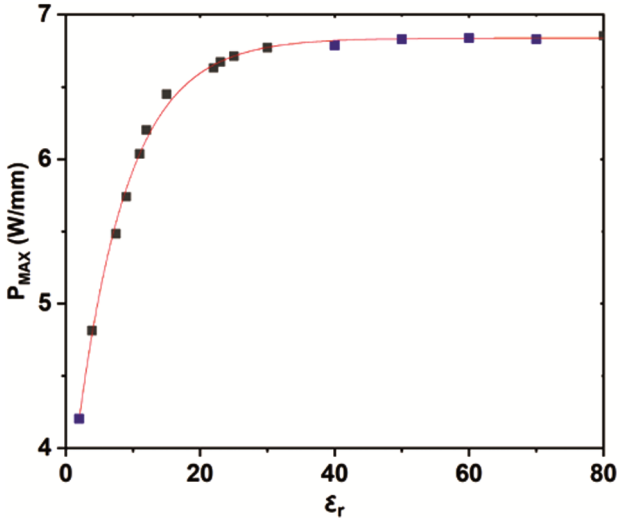

Fig. 7 — Variations of P_{max} as a function of relative permittivity of real (■■■) and fictitious (■■■) materials and line of best fit (——), at V_{GS} = 0 V and V_{DS} = 20 V.

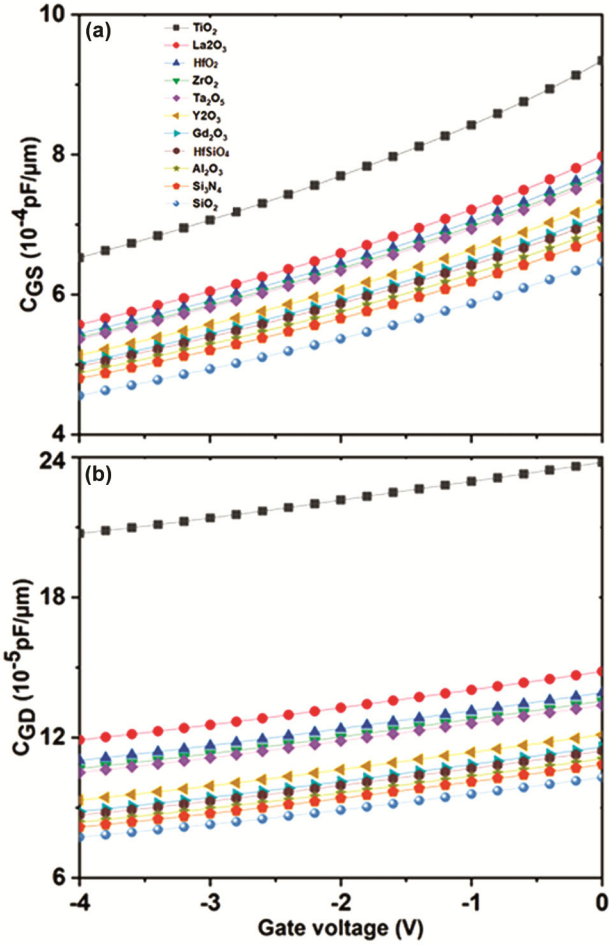

Fig. 8 — Evolution of access capacitances as a function of V_{GS}, (a) C_{GS}(V_{GS}) and (b) C_{GD}(V_{GS}) at a V_{DS}=40 V and a frequency f= 1 GHz for different dielectric layers.

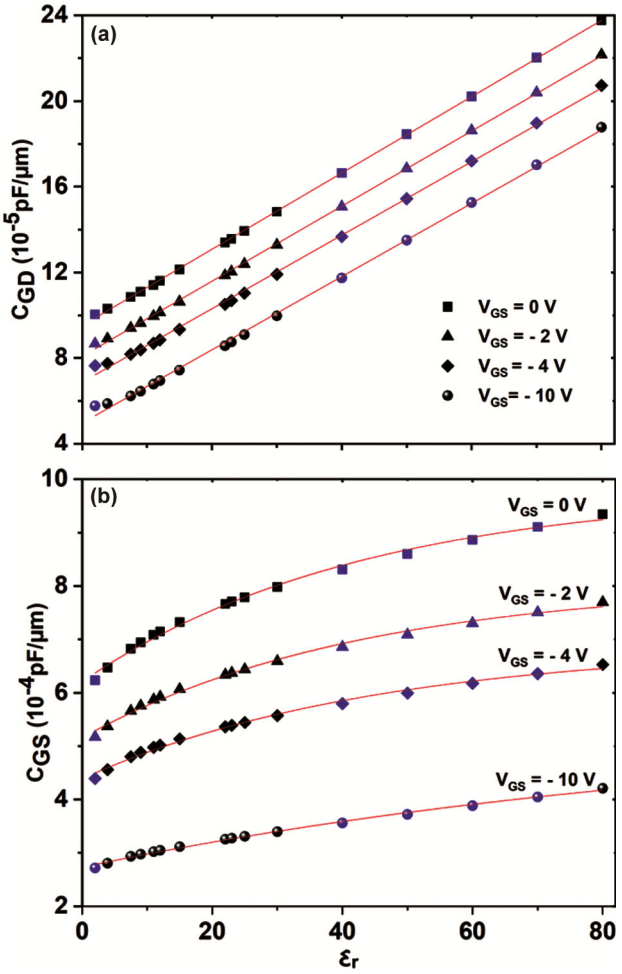

Fig. 9 — Variation of access capacitances as a function of ε_r: (a) $C_{GD}(\varepsilon_r)$ (■ ■) and (b) $C_{GS}(\varepsilon_r)$ (■ ■) at V_{DS} = 40 V, for different V_{GS} values and f = 1GHz and line of best fit (——).

Where β is a characteristic constant that depends on V_{GS} values. Rigorous investigations of several V_{GS} polarizations led to the deduction of β expression:

$$\beta = 9.5 + 0.8V_{GS} + 0.036V_{GS}^2$$

Hence, by introducing β expression into Eq. 5, C_{GD} expression becomes:

$$C_{GD}(10^{-5}pF/\mu m) = 0.18\varepsilon_r + 0.8\,V_{GS} + 0.03\,V_{GS}^2 + 9.5 \quad \ldots (6)$$

For the exponential C_{GS} variations Fig. 9(b), the following expressions were deduced for different V_{GS} values:

at V_{GS} = 0 V : $C_{GS}\left(\frac{10^{-4}pF}{\mu m}\right) = 9.8 - 3.7e^{(-\varepsilon_r/43)}$ …(7a)

at V_{GS} = - 2 V : $C_{GS}\left(\frac{10^{-4}pF}{\mu m}\right) = 8.0 - 2.9e^{(-\varepsilon_r/43)}$ …(7b)

at V_{GS} = - 4 V : $C_{GS}\left(\frac{10^{-4}pF}{\mu m}\right) = 6.9 - 2.5e^{(-\varepsilon_r/45)}$ …(7c)

at V_{GS} = - 10 V: $C_{GS}\left(\frac{10^{-4}pF}{\mu m}\right) = 5.4 - 2.7e^{(-\varepsilon_r/105)}$ …(7d)

Thus, the C_{GS} exponential variations (Eq. 7a-d) can be generalized as follows:

$$C_{GS}(10^{-4}pF/\mu m) = A - Be^{(-\varepsilon_r/C)} \quad \ldots (8)$$

where, A, B and C are characteristic constants that depend on V_{GS} values.

The importance of the above-deduced relations (Eqs. 6 and 7) lies in the fact that C_{GD} or C_{GS} capacitances are expressed in terms of known (or measurable) parameters. Therefore, these capacitances can be deduced by just knowing ε_r and V_{GS}.

7 Conclusions

This investigation concerns the influence of numerous passivation layers (SiO_2, Si_3N_4, Al_2O_3, $HfSiO_4$,Gd_2O_3, Y_2O_3, Ta_2O_5, ZrO_2, HfO_2, La_2O_3 andTiO_2) on the DC and RF properties of GaN MESFET (amplitude and line distribution of electric field, breakdown voltages, gate-source and gate-drain capacitances). The simulations were carried out using ATLAS of Silvaco physical simulator for such devices with variable passivation layers with range of relative permittivity values ε_r (2 to 80). Thus, it was shown that the choice of dielectric passivation layer is of great importance in improving or degrading the device performances. In fact, it has been shown that when the dielectric relative permittivity becomes higher, the electrical field strength is reduced with a less dense field lines. These changes, led to higher breakdown voltage and the improvement of the maximum output power density and consequently the performance of the GaN MESFET for high power device applications

Moreover, the relative permittivity also affects the gate-source and gate-drain capacitances. In fact, for all V_{GS} values, it was shown that for increasing relative permittivity values both C_{GD} and C_{GS} increase. However, the effect of ε_r on C_{GD} was linear while it is exponential on C_{GS}. These variations were quantified, through curve fitting, to deduce the relationships between capacitances and relative permittivity. The

determined semi-empirical relations are of great interest in the direct determination of both C_{GD} and C_{GS} capacitances by just knowing ε_r and V_{GS} and vice-versa.

Finally, the established results show that the choice of passivation layer with high relative permeability leads to better performance in terms of DC characteristics, for high voltage and high power applications of the MESFETs GaN. However, it would be preferable to opt for low permittivity layers to avoid possible degradation of RF characteristics.

Acknowledgment

This research work was supported by the DG-RSDT (MESRS), Algeria, under PRFU programs.

References

1 *Soma* U, *Silicon*, 14 (2022) 9669.
2 Balaji B, Rao K S, Aditya M & Sravani K G, *Silicon*, 14 (2022) 8449.
3 Hamma I, Ziar T, Farh H, Saidi Y & Azizi, C, *Optik*, 233 (2021) 166479.
4 Khoorabeh M, Orouji A A & Madadi D, *Silicon*, 14 (2021) 2757.
5 Tanaka R, Takashima S, Ueno K, Matsuyama H & Tanaka M, *Jpn J Appl Phys*, 59 (2020) SGGD02.
6 Sun M, Zhang Y, Gao X & Palacios T, *IEEE Electron Dev Lett*, 38 (2017) 509.
7 Ohta H, Asai N, Horikiri F, Narita Y, Yoshida T & Mishima T, *IEEE Electron Dev Lett,* 41 (2019) 123.
8 Godfrey D, Nirmal, D, Godwinraj D, Arivazhagan L, MohanKumar N, Tzou J & Yeh W K, *Silicon,* 13 (2021) 1177.
9 Maeda T, Narita T, Ueda, H, Kanechik M, Uesugi T, Kachi T, Kimoto Y, Horita M & Suda J, *IEEE Int Electron Dev Meeting,* 18-687 (2018).
10 Arabshahi H, *Braz J Phys*, 39 (2009) 35.
11 Hamma I, Ziar T, Farh H, Saidi Y & Azizi C, *Optik*, 233 (2021) 166479.
12 Rehman S U, Ahmed U F, Ahmed M M & Khen M N, *IEEE Access*, 7 (2019) 49702.
13 Doundoulakis G, Adikimenakis A, Stavrinidis A, Tsagaraki K, Androulidaki M, Iacovella F, Deligeorgis G, Konstantinidis G & Georgakilas A, *Nanotechnol*, 30 (2019) 285304.
14 Atlas (2012) User's Manual: 2-D Device Simulator, Santa Clara,CA, USA.
15 Prasanna K S, Sandeep P, & Choudhary S, *Superlattics Microstruct,* 111 (2017) 642
16 Lenka T R & Pandapramana A K, *Pramana-J Phys,* 79 (2012) 151.
17 Robertson J, *Eur Phys J Appl Phys*, 28 (2004) 265.
18 Yatabe Z, Asubar J T & Hashizume T, *J Phys D: Appl Phys*, 49 (2016) 393001.
19 Dal F P A, Kayal M, *Linear CMOS RF power amplifiers for wireless applications*, Springer Dordrecht, (2010).
20 Mishra U K & Singh J, *Semiconductor device physics and design*, Springer, Dordrecht, (2008)
21 Abid L, Hadjoub I, Doghmane A, Abdaoui N E & Hadjoub Z, *Silicon*, 14 (2022) 11605.